European Journal of Medicinal Chemistry 58 (2012) 192–205

Contents lists available at SciVerse ScienceDirect

European Journal of Medicinal Chemistry

journal homepage: http://www.elsevier.com/locate/ejmech

Original article

Novel peptidomimetic compounds containing redox active chalcogens and quinones as potential anticancer agents

Saad Shaaban [a,c], Randi Diestel [a], Bettina Hinkelmann [a], Yazh Muthukumar [a], Rajeshwar P. Verma [b], Florenz Sasse [a,*], Claus Jacob [c,**]

[a] Department of Chemical Biology, Helmholtz Centre for Infection Research, Inhoffenstraße 7, D-38124 Braunschweig, Germany
[b] Department of Chemistry, Pomona College, 645 North College Avenue, Claremont, CA 91711, USA
[c] Division of Bioorganic Chemistry, School of Pharmacy, Saarland University, Campus B2.1, D-66123 Saarbrücken, Germany

ARTICLE INFO

Article history:
Received 5 August 2012
Received in revised form
22 September 2012
Accepted 25 September 2012
Available online 4 October 2012

Keywords:
Oxidative stress
Multicomponent reactions
Passerini reaction
Anticancer activity
Chemogenomic assay

ABSTRACT

Many types of cancer cells are associated with a disturbed intracellular redox balance and oxidative stress (OS). Among the various agents employed to modulate the intracellular redox state of cells, certain redox catalysts containing quinone and chalcogen moieties have shown considerable promise. Passerini multicomponent reaction has been developed for the synthesis of agents combining two, three or even four redox centers in one molecule in a good yield. When incubated with cancer cells these agents inhibited cell proliferation and induced apoptotic cell death. Interestingly, some of these redox active compounds exhibited quite low toxicity with normal cells. The cause was obviously OS, which was reflected by significant decrease in reduced glutathione, subsequently cell cycle arrest and induction of apoptosis.

1. Introduction

Therapeutic selectivity and drug resistance are two major issues in cancer chemotherapy. By targeting the genetic differences between normal and cancer cells, drugs like Gleevec and Herceptin show promising therapeutic activity and few side effects [1]. These gene-targeting strategies however, are still facing problems because of acquired drug resistance and genetic instability of cancer cells [2]. Recent studies suggest that targeting the particular biochemical alterations, biochemical signature, in cancer cells might be a feasible approach to develop a cancer therapy that does not lead to the development of drug resistance [3].

Many types of cancer cells show a disturbed intracellular redox balance, making them different from their healthy counterparts. Some tumors, such as solid lung carcinoma, are hypoxic, *i.e.*, their cells are more reducing than normal ones, while others, such as the cells of prostate and breast cancer are naturally under oxidative stress (OS). When compared to healthy cells, their reactive oxygen species (ROS) levels are considerably closer to the critical redox threshold at which cell death is induced [4]. These biochemical differences between healthy and malignant tissue are significant, and can be used to design selective, yet effective redox drugs [5,6].

Several avenues have therefore been explored during the last ten years to use the naturally occurring OS to selectively kill cancer cells. Currently explored ROS-inducing strategies can be divided into three main lines of investigation: i) agents that directly increase ROS in cancer cells to lethal levels (ROS-generators), ii) agents that inhibit antioxidant enzymes and hence raise ROS concentrations to lethal levels, and iii) catalysts that enhance the toxicity of pre-existing ROS (ROS-users and ROS-enhancers) [4,7]. ROS generators and inhibitors of antioxidant defense systems (strategies i and ii) add an additional ROS burden without really discriminating directly between normal and sick cells. They rely only on the pre-existing differences in basal ROS levels between cancer and normal cells. Furthermore, the dosage of such agents is a serious problem. These compounds are not catalytic, and therefore need to be administered in rather large quantities, which might lead to serious side effects. In contrast, catalytic molecules (strategy iii) that employ ROS as their substrates may not only raise ROS levels, but they may also exhibit selectively in cells rich in ROS, without exhibiting the same chemistry in normal cells. Although some of these agents may exhibit selectivity to cells rich in ROS,

* Corresponding author. Tel.: +49 531 6181 3428; fax: +49 531 6181 3499.
** Corresponding author. Tel.: +49 681 302 3129; fax: +49 681 302 3464.
E-mail addresses: florenz.sasse@helmholtz-hzi.de (F. Sasse), c.jacob@mx.uni-saarland.de (C. Jacob).

0223-5234/$ – see front matter © 2012 Elsevier Masson SAS. All rights reserved.
http://dx.doi.org/10.1016/j.ejmech.2012.09.033

they are not able to efficiently eliminate cancer cells that have become adapted to stress. This may be due to the fact that a disturbed redox balance is not just due to one chemical species but is the result of a combination of various ROS and reactive nitrogen species, metal ions, and deficiencies in antioxidant defenses. Having the above facts in mind and in continuation of our earlier efforts to synthesize agents that increase ROS selectively in cancer cells to lethal levels, we were interested to synthesize agents containing both ROS-generating and ROS-using moieties in one molecule.

A combination of ROS-modulators is required to effectively eliminate cancer cells and is expected to maximally exploit the ROS-mediated cell-death mechanism as a therapeutic strategy. This approach is adopted to increase the catalytic efficiency and might be particularly useful in cells that have become adapted to stress and are therefore resistant to traditional anticancer agents.

As part of our present study, we have therefore explored the effective synthesis of multifunctional redox modulators and used these agents to perform a comprehensive cell biological analysis of the potential mode of biochemical action. Combining an in depth analysis of whole cell behavior (cell morphology, cell cycle arrest, induction of apoptosis) with biochemical changes (ROS and GSH levels, caspase activity) and a modern chemogenomic approach, we are able to confirm the suspected redox link which ultimately is the most likely explanation for some of our compound's selective activity against certain cancer cells under (pre-existing) OS.

2. Results and discussion

2.1. Chemistry

The desire to increase the efficiency and selectivity for cancer cells under OS has required the synthesis of complicated redox modulators which are tailored to recognize the biochemical redox signature of OS in cancer cells. These agents often combine three or even more functionalities (redox centers, metal binding sites) in one molecule and therefore may act efficiently and selectively against those cells [8]. Recently we have reported compounds containing two, three or even four redox sites in one molecule. These molecules were efficient in sub-micromolar concentrations *i.e.*, at rather low concentrations [9,10]. Based on these results, we were interested to further conduct an extensive antitumor screen using a variety of novel multi-redox compounds in order to obtain evidences regarding the structural requirements underlying the cytotoxicity/selectivity of ROS-generators, ROS-users and/or ROS-enhancers when they are combined together.

2.1.1. The multicomponent Passerini reaction as a key to multifunctional redox agents

Our design strategy relies on the combination of quinones as ROS-generators, organochalcogens as ROS-users, and/or porphyrin as ROS-enhancers. The synthesis of such compounds encounters increasing difficulties when moving from just one or two to three or more redox sites. The synthesis of chalcogen based quinone agents has often been marred by low yields, decomposition of the products and difficulties to generate compounds in sufficient quantities and purities. Even the most basic, bi-functional agents have been difficult to obtain [11–13]. These problems in turn have hindered the development of multifunctional redox catalysts. Therefore, the development of a multicomponent one-step synthetic method using stable reagents under neutral conditions has attracted our attention. The Passerini three-component reaction (P-3CR) in the context of diversity-oriented synthesis has been used to achieve high levels of diversity and brevity. The design of new combinations of simple and flexible building blocks gave rise to novel and diverse complex structures by simultaneous formation of two or more bonds, according to the domino and divergence principles [14,15].

Apart from being able to successfully deliver highly complicated, multifunctional redox catalysts, the P-3CR employed here is characterized by two additional aspects. From the perspective of organochalcogen chemistry, the yields obtained by this method vary from 62% to 93%, *i.e.*, they are generally quite good as far as organoselenium compounds are concerned (Table 1).

Furthermore, the P-3CR was performed under different conditions using different solvents. The best results in terms of reaction time and yield were obtained when the reaction was performed in the presence of water and under mild conditions (room temperature) [16,17]. Moreover, not only does the use of water as solvent permit the reaction to be conducted rapidly, the products are often insoluble, facilitating their ready isolation. Although mixed aqueous solvents are popular as a medium for MCRs and related chemistry, the use of pure water without any co-solvents seems to be an exception to the rule [16]. This could be attributed to many factors, including the hydrophobic effect and enhanced hydrogen bonding in the transition state.

2.1.2. Building blocks used in the P-3CR

The P-3CR described here required a range of building blocks, which needed to be designed and synthesized first. Fig. 1 provides an overview of the various aldehydes, acids, and isonitriles used.

Although the synthesis of appropriate quinone- and chalcogen-bearing building blocks is not always straight forward, a range of such compounds have now been reported by us in the literature [9,10]. Of particular importance is the bifunctionalized quinone–selenium bearing aldehyde (**1c**) and the quinone–sulfur bearing acid (**2b**). Other building blocks were chosen to incorporate the amino acid residues of glycine, L-serine, and cysteine to the product backbone for biological and pharmacological reasons (**2c**–**2e**).

In case of the isonitrile building blocks, **3b** was used in addition to the commercially available but expensive *tert*-butyl isonitrile (**3a**) which is frequently used. In most cases **3b** offers superior

Table 1
Building blocks, solvents, and yields of the synthesis of compounds **4**–**18**. Building blocks were designed to carry one or two relevant redox or metal binding sites, which could be combined to larger, highly functionalized molecules with four or more biologically interesting sites. Reactions were mostly performed in water at high concentrations and under mild conditions.

Cpd. no.	Building blocks	Solvent	Yield (%)	Redox centers	Cpd. no.	Building blocks	Solvent	Yield (%)	Redox centers
4	1b, 2b, 3a	H_2O	62	3	**12**	1c, 2d, 3b	H_2O	75	2
5	1a, 2b, 3a	H_2O	68	3	**13**	1c, 2c, 3b	H_2O	66	2
6	1a, 2b, 3b	H_2O	71	3	**14**	1c, 2e, 3b	H_2O	85	4
7	1c, 2b, 3a	H_2O	76	4	**15**	1c, 2a, 3b	H_2O	79	3
8	1b, 2b, 3b	H_2O	75	3	**16**	1d, 2f, 3a	$CHCl_3$	93	1
9	1c, 2b, 3b	H_2O	73	4	**17**	1a, 2f, 3a	$CHCl_3$	89	2
10	1c, 2d, 3a	H_2O	76	2	**18**	1c, 2f, 3a	$CHCl_3$	86	3
11	1c, 2e, 3a	H_2O	54	4					

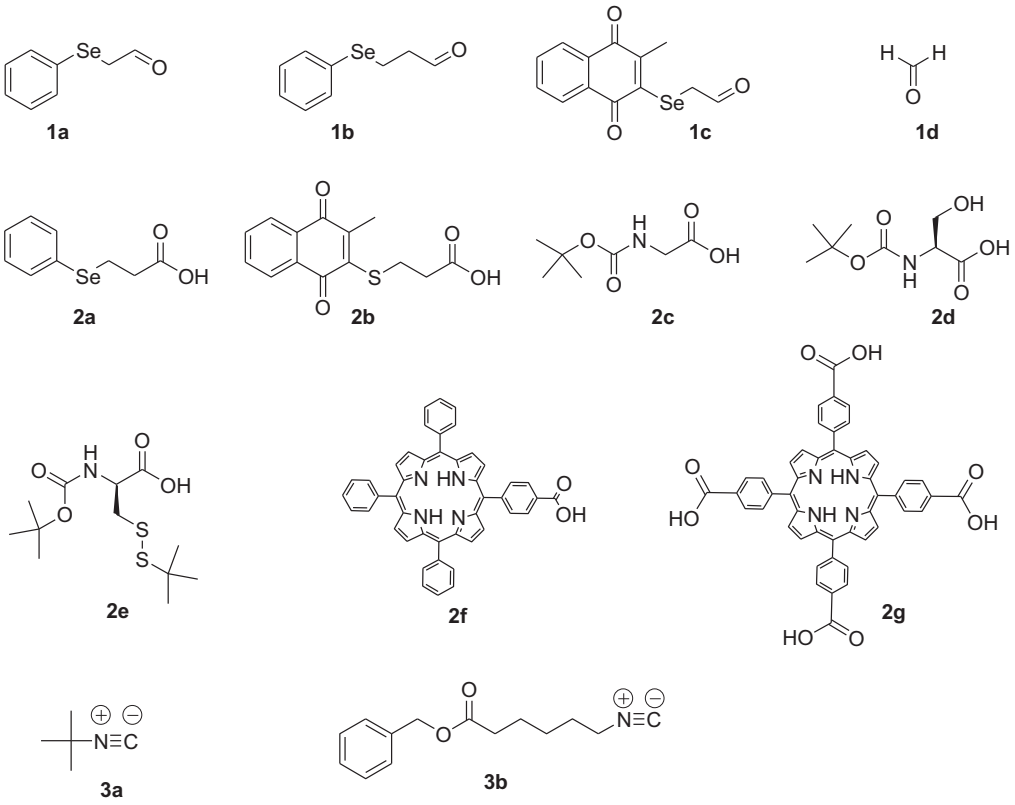

Fig. 1. Building blocks used to synthesize multifunctional redox agents. Acid, aldehyde and isonitrile building blocks used in the Passerini reaction were synthesized following literature procedures or, in case of hitherto unknown agents, could be synthesized in sufficient yield.

reactivity compared to **3a**. Furthermore, **3b** adducts can undergo further derivatization [18].

All the building blocks required were synthesized following literature procedures or, in case of hitherto unknown agents, were synthesized in sufficient yield and purity. Analytical information is given in the Supplementary material.

2.1.3. Synthesis of selected multifunctional redox agents

Our main objectives are to exploit the 'mix and match' design criteria to synthesize a small library of chemically diverse compounds able to target cancer cells under oxidative stress using simple and efficient synthetic procedure. In order to turn the hits into lead compounds, this library thereafter will be submitted to *in vitro* evaluation. Therefore a library of 15 chemically diverse compounds (**4**–**18**) (Fig. 2) was synthesized using P-3CR. Large libraries accordingly are planned to be synthesized after obtaining evidences regarding the structural requirements underlying the cytotoxic/selective behavior of our representative library.

Compounds were synthesized in order to combine diverse redox centers: A) compounds possessing two redox centers of which one is quinone and one is selenium (**10**, **12**, **13**); B) compounds possessing three redox centers, either with one quinone, one selenium and one sulfur (**4**, **5**, **6**, **8**), or with one quinone and two selenium (**15**), or with one quinone, one selenium and disulfide moiety (**11**,**14**); C) compounds possessing four redox centers with two quinones, one selenium and one sulfur moieties (**7**, **9**). Furthermore, compounds containing a porphyrin metal binding center with/without chalcogen and quinone redox sites were also synthesized. These compounds contain: A) only a metal binding porphyrin center (**16**); B) a metal binding porphyrin center and selenium redox center (**17**); and C) a metal binding porphyrin center, one quinone and selenium redox center (**18**).

2.2. Pharmacology

Naphthoquinones, particularly 1,4-naphthoquinone, utilize several mechanisms to exert a cytotoxic effect [19,20]. Of special interest is their ability to redox cycle with triplet oxygen, forming superoxide and peroxide capable of inflicting damage (ROS generators) [21–23]. In contrast, organoselenium compounds (so called ROS-users), mimicking the catalytic cycle of the selenoenzyme GPx, are able to use ROS and speed up reactions with redox-sensitive proteins and enzymes, ultimately causing malfunction and cell death [24]. Furthermore, metalloporphyrins (ROS-enhancers) are able to convert less reactive and damaging ROS, such as $O_2^{\bullet-}$, to more damaging species, such as the highly aggressive hydroxyl ($^{\bullet}OH$) radical [25,26].

In theory, the ROS-generating and the ROS-using centers complement to each other. The peroxide formed as a result of redox cycling of the quinone moiety has the ability to induce cellular injury and, at the same time, to activate the chalcogen/porphyrin moieties, which in turn are responsible for the oxidation of redox-sensitive proteins and enzymes leading to oxidative damage. Importantly, such multifunctional compounds have not been fully tested before in a cancer cell screen and therefore may provide a truly new lead for compound development.

2.2.1. Cytotoxic activity of redox active compounds in cancer cells and healthy cells

In order to check if any of the multifunctional agents may be useful for further biochemical investigations, a one-dose screen of compounds **9**, **10**, **12**, and **14** was performed at the National Institute of Health (NIH) in Bethesda, MD, USA. This screen includes 58 cell lines grouped into breast cancer, renal cancer, colon cancer,

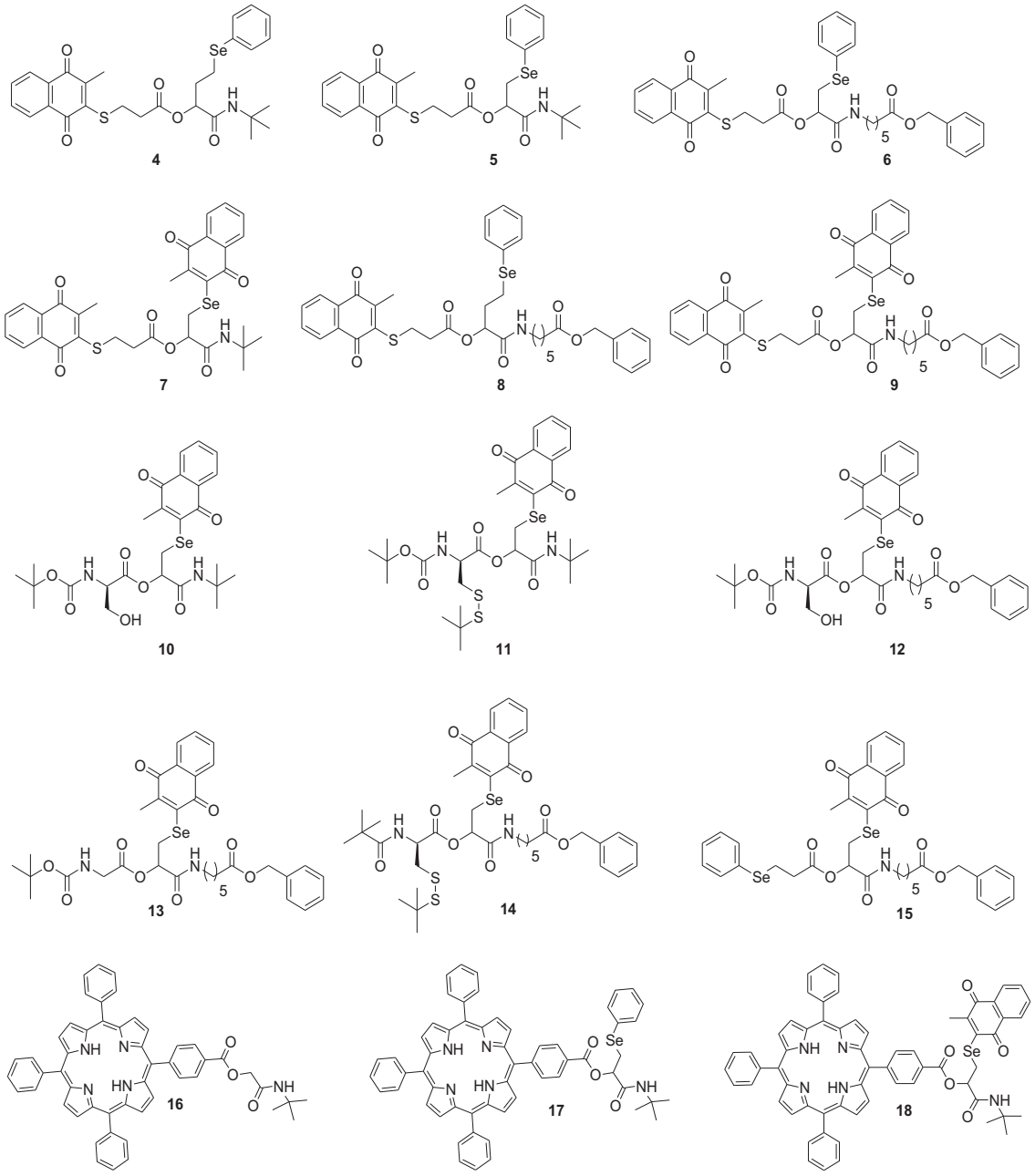

Fig. 2. The Passerini multicomponent reaction was used for the synthesis of di-, tri- and tetra-functional redox agents **4**–**18** containing multiple chalcogen and quinone redox sites.

prostate cancer, ovarian cancer, CNS cancer, non-small-cell lung cancer, leukemia, and melanoma cell lines.

Interestingly, all the compounds tested exhibited a significant cytotoxicity against cancer cell lines and were subsequently selected for 5-dose testing. GI_{50} values were in the low to sub-micromolar range (Supplementary material). COMPARE analyses were performed using the correlation coefficient method. The compounds' pattern activities correlate with cisplatin which is used to treat various types of cancers, including sarcomas, lymphomas, and germ cell tumors, and methyl mitomycin C which has an antitumor antibiotic activity against breast cancer, and last but not least with anthracycline-based redox agents representing menogaril, deoxydoxorubicin, and MX2 HCl, which are used in the treatment of prostate cancer and leukemia (Supplementary material).

Based on the above promising results, the cytotoxic activity of the test compounds was further assayed in details with different cancer cell lines, *i.e.*, MCF-7 (human breast adenocarcinoma), A-498 (human kidney carcinoma), and A-431 (human epidermoid carcinoma). Cells were incubated with serial dilutions of the compounds, and the metabolic activity measured by means of an MTT assay after 24 h and the IC_{50} values are estimated from the dose–response curves (Table 2).

Interestingly, we found a correlation between chemical structures and toxic activities. Compounds **7** and **9** with four redox centers are more cytotoxic than their homologs with two and three redox centers as was expected. Furthermore, the most toxic compounds **7**, **9**, **10**, **12** and **14** posses a direct attachment of the selenium to the quinone, in contrast to the structurally similar get less toxic compounds **4**, **5**, **6** and **8**, where the selenium atom is located further away from the

Table 2
Influence of multifunctional redox compounds **4**–**18** on the viability of human cancer cells and normal cells.

Cpd. no.	MCF-7[b]	A-498[b]	A-431[b]	HUVEC[a]	HF[a]	Cpd. no.	MCF-7[b]	A-498[b]	A-431[b]	HUVEC[a]	HF[a]
	IC_{50} (μM)						IC_{50} (μM)				
4	26	>100	>100	13	11	**12**	5	5	4	35	27
5	14	>100	7	34	26	**13**	4	7	5	36	6
6	10	>100	>100	23	50	**14**	8	13	4	10	4
7	3	3	1	1	n.d.	**15**	9	4	4	3	6
8	19	>100	>100	17	21	**16**	>100	>100	>100	>100	>100
9	10	5	6	7	5	**17**	>100	>100	>100	>100	>100
10	3	5	2	3	7	**18**	>100	>100	>100	>100	>100
11	3	5	2	2	4						

The metabolic activity of the cells was measured after one day of incubation with different concentrations of the test compounds by means of an MTT assay. The IC_{50} was determined from the dose–response curves as the mean of two parallel experiments; b cancer cell line; a primary cells; n.d. not detected.

quinone moiety. But there were exceptions: compounds **10** and **12** with only two redox centers were also among the most active compounds. On the other hand, compounds **16**, **17** and **18** with a metal binding porphyrin site showed no cytotoxic effect in the concentration range tested ($IC_{50} > 100$ μM) even though compound **18** contains two additional redox centers (quinone and selenium).

When incubated with primary human fibroblasts (HF) and human umbilical vein endothelial cells (HUVEC) most of the test compounds had a toxic effect with the exception of compounds **5**, **6**, **12** and **13** (Table 2). Compound **12** clearly showed lower cytotoxicity against both primary cells than against the three cancer cell lines under investigation. The same holds true for **13** with the exception that it was toxic to HF cells. Compound **5** showed higher activity against breast and epidermoid cancer cells while compound **6** showed higher toxicity against breast cancer but not against epidermoid cancer cells. These compounds share almost the same chemical features and this might be the reason for their selective anticancer behavior. Compounds **6**, **12** and **13** possess the same hydrolyzable benzylhexanoate ester side chain and have a comparable molecular weight (707, 730, and 700 g/mol, respectively). Compounds **5** and **6** have three redox centers, compounds **12** and **13** two redox centers each. Importantly, all these compounds combine a quinone with a selenium redox center. Such specific molecular features might be the reason for the selectivity of the compounds.

2.2.2. Assessment of OS induction

Quinones and organochalcogens, each separately, have been shown to be cytotoxic *via* various mechanisms. The exact mechanism by which chalcogen based quinones exhibit their cell killing effect, however, remains to be explored. Previously, we have investigated the GPx like catalytic activity of the multifunctional redox agents using a thiophenol-based (PhSH) assay [9]. The results obtained, at that time, showed that several compounds were even more active than the benchmark compound ebselen [9]. We also reported that these compounds had no tangible antioxidant activity (which may be counter-productive). This was confirmed with the thiobarbituric acid assay, where most of the compounds were not particularly active [9].

In continuation to our previous work, the notion that the multifunctional agents might be toxic *via* increasing the severity of OS was further investigated. The GSH level in addition to the intracellular levels of ROS (*e.g.*, $O_2^{\bullet-}$ and H_2O_2), upon treatment with different concentrations of the test compounds, were assessed spectrophotometrically with specific probes, *i.e.*, 5,5′-dithiobis (2-nitrobenzoate) (DTNB), 2′,7′-dichlorodihydrofluorescin diacetate (DCF), and dihydroethidium (DHE).

2.2.3. GSH assay

Low levels of GSH are linked to mitochondrial dysfunction and induction of apoptosis, thus decreasing chemoresistance [27–29]. Therefore, the intracellular levels of reduced glutathione were estimated by the DTNB assay.

The DTNB assay is fairly specific for GSH and allows the determination of GSH concentrations in the presence of other intracellular thiols [20]. Fig. 3 shows that the GSH levels were reduced when the cells were incubated with different redox active compounds. After 1 h, a concentration of 5 μM of compounds **11**, **10**, **15**, and **13** caused a decrease of the intracellular GSH level in MCF-7 cells by 46%, 59%, 62%, and 76%, respectively. These observations are consistent with a recently reported study where several quinone-containing compounds, with anticancer property, exert their activity *via* depletion of GSH [27–29].

2.2.4. Measurement of intracellular ROS levels

The mediation of OS *via* the production of $O_2^{\bullet-}$ and H_2O_2 needed to be further investigated. The DCF and DHE assays are considered to be general indicators of ROS. DCF reacts with H_2O_2, $ONOO^-$, and lipid hydroperoxides. It is cell permeable, and after uptake is cleaved by intracellular esterases to the non-fluorescent 2′,7′-dichlorofluorescin (DCFH) which is trapped within the cells. DCFH could be oxidized by a variety of ROS to the fluorescent 2′,7′-dichlorofluorescein (DCF) which can be detected on fluorescence spectrophotometer [30].

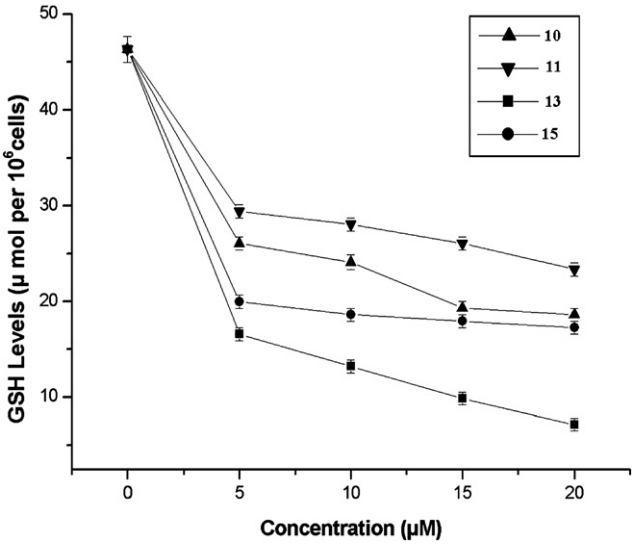

Fig. 3. Assessment of the intracellular levels of reduced glutathione in breast cancer cells. Depletion of the intracellular levels of reduced GSH in MCF-7 cells treated with compounds **10**, **11**, **13**, and **15** for 1 h were assessed employing the DTNB assay which is fairly specific for glutathione.

The DHE assay is close to being a gold standard method for detecting $O_2^{\bullet-}$ [31]. DHE is a lipophilic probe that readily diffuses across plasmatic membranes. Once inside the cell, it is rapidly oxidized by $O_2^{\bullet-}$ to the red fluorescent 2-hydroxyethidium. The later is trapped in the nucleus by intercalating into DNA, leading to an increase of fluorescence.

Compounds under investigation were able to significantly increase the intracellular ROS levels in A-431 cells (Fig. 4, panel a and panel b). The ROS formed as a result of redox cycling of the quinone moiety are sufficiently potent to damage cells and have the potential to activate the chalcogen center(s) of the catalyst. The chalcogen redox center(s), in turn, are able to oxidize redox-sensitive thiol groups in proteins and enzymes, ultimately causing malfunction and cell death. Thiol oxidation catalysis is, however, highly detrimental to the cell, which could explain the high toxicity of such chalcogen-based compounds.

In theory, an ideal anticancer agent should be toxic to malignant cells with minimum toxicity in normal cells. Within this context, the levels of ROS of A-431 cells were monitored in comparison with HUVECs. Fig. 5, panel a and panel b show that A-431 cells have higher basal levels of ROS compared to HUVECs. Importantly, compounds **4**, **8**, **9** and **11** were able to increase the intracellular ROS level in melanoma cells to a greater extent than in HUVECs.

This behavior points to a specific kind of selectivity, supporting the notion that exploiting the biochemical differences between normal cells and cancer cells might lead to the development of new selective anticancer agents able to overcome the challenges facing current therapeutic strategies [3]. Although it is too early to speculate about possible uses of such catalytic, multifunctional redox agents in therapy, their activity and selective cytotoxicity against certain cancer cells encourages the further investigation of catalytic agents as potential anticancer drugs.

2.2.5. Phenotypical changes in cellular morphology, cytoskeleton, and endoplasmic reticulum

OS induces cellular injury by the production and accumulation of highly reactive free radicals. This may cause increased plasma-membrane permeability and peroxidation, release of cytosolic components, disassembly of the cytoskeleton, and damage to all types of cellular biomolecules, including DNA, proteins and lipids [32–34]. Within this context, we used fluorescence techniques to look for phenotypical changes in the cytoskeleton architecture, the nucleus, and the morphology of the endoplasmic reticulum of potoroo cells (PtK2).

Fig. 6 shows that the ER structure is affected by the redox modulators (typical ER stress) and that the cell morphology in general is altered; cells are rounded, and detached from each other. The adhesion of the cells seems to be reduced and actin stress fibers are barely detectable. On the other hand, no phenotypical changes were noticed in case of the microtubular network (not shown).

The cytoskeleton may represent one of the preferential targets of ROS whatever OS is applied due to its structure. Indeed, cytoskeletal proteins are particularly abundant within the cells and several protein constituents of the cytoskeleton display highly reactive residues that can be easily oxidized. Hence, the actin cytoskeleton is considered to be an early target of cellular OS [35]. The later causes disruption of the normal organization of microfilaments essentially due to oxidative modifications of specific cysteine thiols and methionine sulfides of actin [29,36,37]. Although the interplay between the OS and ER stress is not clear, both of them have been implicated in the pathogenesis of a wide variety of diseases, such as neurodegenerative disorders, diabetes and ischemia reperfusion heart disease [38].

2.2.6. Cell cycle and apoptosis

Examination of the current literature on the effect of OS on the cell cycle reveals that increases in ROS-induced DNA damage are correlated with cell cycle arrest. For instance, Upadhyay et al. recently described that a sublethal dose of H_2O_2 prevents progression of cell cycle by causing delay in G0/1 [39]. The same behavior was observed with our multifunctional redox agents. A significant delay of cell cycle progression was observed when MCF-7 cells were treated with **10**, **11** and **15** at their respective IC_{50} concentrations for 24 h. A clear reduction of cells in G2/M phase and an increase in the G0/1 phase compared to methanol treated cells (negative control) were observed (Fig. 7).

It has been reported that high levels of ROS can induce apoptosis by activating either the ER stress-mediated apoptotic pathway or the mitochondrial-mediated apoptotic pathway or by activating both pathways. The elevation of cytosolic Ca^{2+}, due to ER stress, may trigger the mitochondrial permeability transition pore opening, cytochrome *c* release, caspase cascade activation, and apoptosis [33,40].

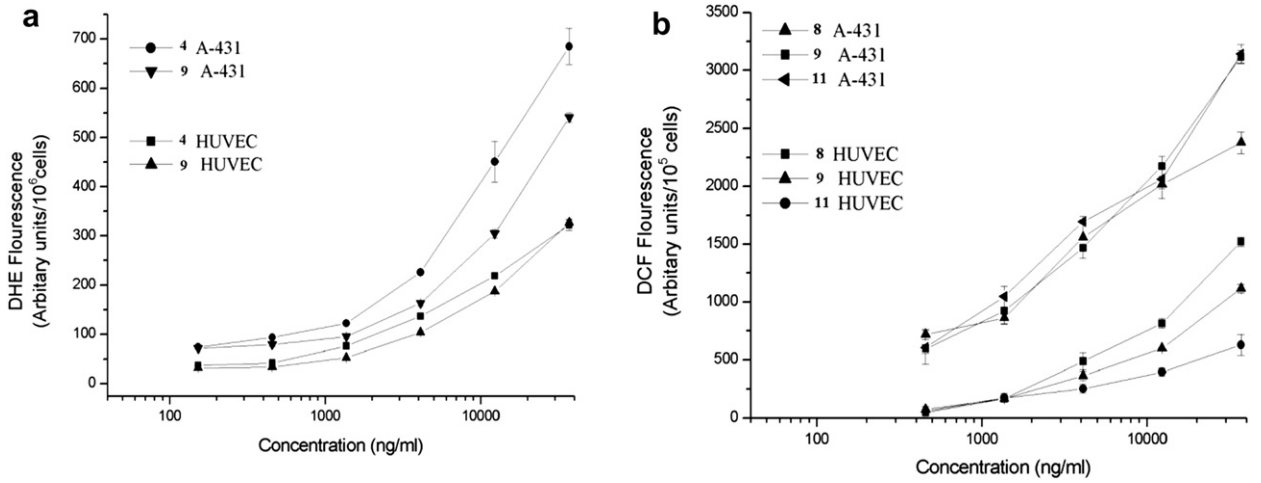

Fig. 4. Assessment of oxidative stress in melanoma and normal human umbilical vein endothelial cells. Using two different methods ROS levels were measured in A-431 in comparison with HUVECs after 1 h of treatment with different concentrations of multifunctional compounds. a) A DCF assay was run after incubation with **8**, **9**, and **11**, b) a DHE assay was performed after incubation with **4** and **9**.

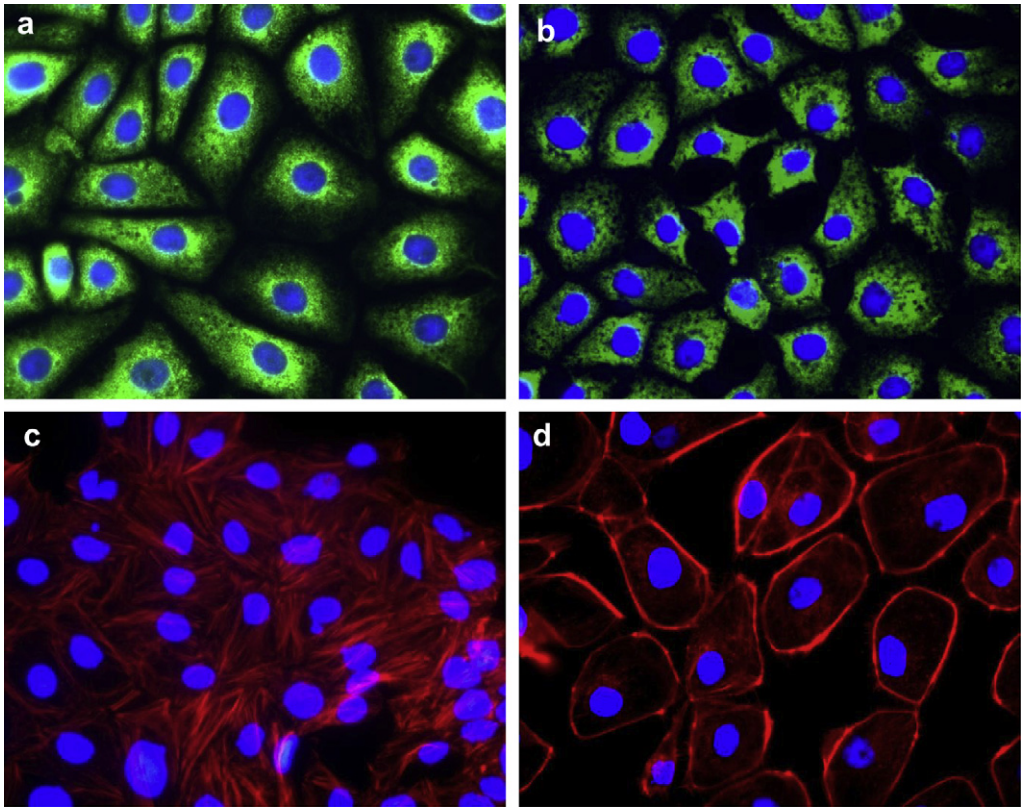

Fig. 5. Immunofluorescence investigations of the ER (panel a and b) and the actin cytoskeleton (panel c and d) of PtK2 cells that were incubated with **10** and **9**, respectively, in comparison with control cells. Compared to the control cells (panel a and c), treated cells show holes in the ER (panel b) and reduced stress fibers (panel d). Cells are rounded and detached from each other.

In general, all apoptotic pathways depend on activation of caspases, in particular effector caspase-3 and -7, for the final execution of apoptosis. Therefore, it might be reasonable to first check these two caspases as a sign of apoptosis. Within this context, the assessment of caspase-3/7 activity in A-431 cells showed a strong activation after 24 h of treatment with compound **15** at a concentration of 2.8 μM (see Supplementary material). The induction of apoptosis was further investigated by flow cytometry after staining the cells with Annexin V and PI. Externalization of phosphatidylserine (PS) to the outer leaflet from the inner leaflet of the plasma membrane is a hallmark of early apoptosis. The FITC labeled Annexin V binds to PS in the presence of Ca^{2+}, resulting in green fluorescence of apoptotic cells. In later stages of apoptosis, PI enters the cells and bind to cellular DNA, resulting in red and intense green fluorescence with Annexin V. As shown in Fig. 7, treatment of A-431 cells with **15** for 12 h resulted in an increase in the percentage of Annexin V (+) (lower right quadrant) and PI (+) (upper right quadrant) cells indicative of apoptosis in a dose dependent manner. The appearance of late apoptotic cells was predominantly (12.9–29.3%) seen at the higher concentrations (13 μM) of **15**. These results were similar to the findings of Kalyanaraman et al., where adriamycin (an anthracycline drug used in cancer chemotherapy) induces apoptosis [41].

2.2.7. Chemical genetic interaction approach

Chemogenomic assays using a mutant library of *Saccharomyces cerevisiae* have proven to be a powerful means to study and predict the mode of action of bioactive compounds. These assays rely on comparing the growth of each gene deletion strain to the wild type strain in the absence and presence of the compounds. The growth inhibition of deletion strains upon exposure to compounds is resulting in a chemical–genetic interaction profile. Analyzing such profiles provides valuable information (*e.g.*, about the pathways and targets that are addressed by new compounds) which is not revealed by conventional methods that easily [42]. We applied a five-step strategy to possibly link the multifunctional compounds to their target pathways: i. We screened all the multifunctional compounds using an agar diffusion assay against *S. cerevisiae* wild type (BY4741) and four mutants (YJR104C, YHR008C, YHR106W and YLR011W), which were chosen because we already know that the genes knocked out in these mutants might be important to counterbalance OS (see Supplementary materials for more details). ii. The IC_{50} values of compounds **10** and **15** (the most active compounds) were determined using a serial-dilution assay against the sensitive mutants YJR104C and YHR008C. iii. Compounds **10** and **15** were then screened against a set of ~4800 viable *S. cerevisiae* deletion strains using the IC_{90} concentration found in step ii. iv. We identified a set of mutants which were sensitive in two chemical–genetic interaction screening procedures (step iii). v. The results from the chemical–genetic interaction profiling were evaluated and confirmed using an agar diffusion assay in a second round of analysis.

At the concentrations applied the compounds under investigation had no effect on the wild type strain, BY4741, but striking effects were observed with ten mutants (Table 3). Superoxide dismutase (mitochondrial (SOD2) and cytosolic copper–zinc (SOD1)), glutathione synthetase (GSH2) and transferase (GTT2), and cytochrome *c* oxidase (COX17) deficient strains were among the most sensitive mutants regarding the test compounds. These enzymes play a major role in the antioxidant defense system and are pivotal for the removal of toxic oxidants. Deletion of the respective genes therefore might cause an OS sensitive phenotype of the mutant. These observations

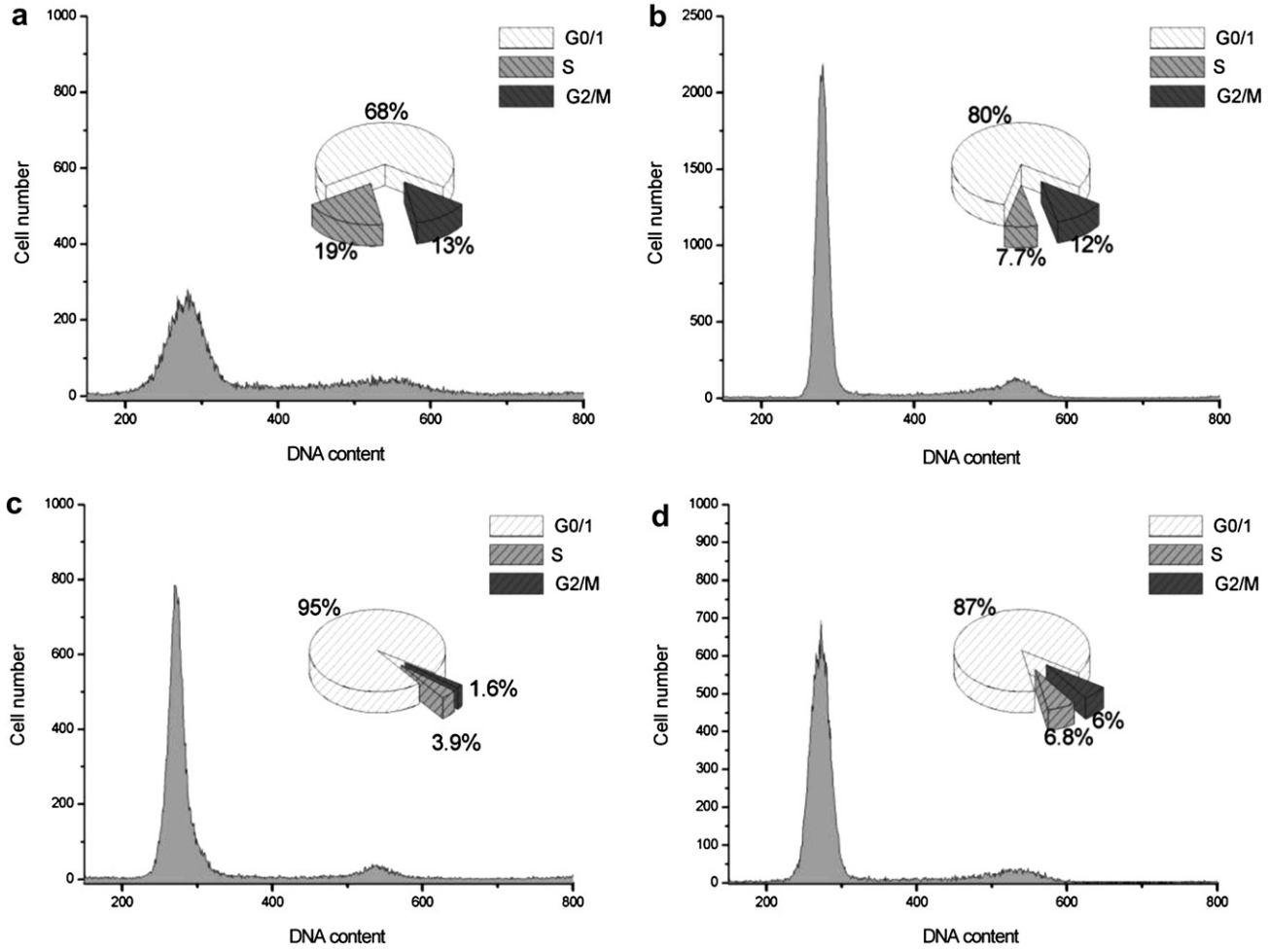

Fig. 6. Cell cycle analysis of MCF-7 breast cancer cells that were treated with methanol (vehicle control; panel a), or with **10** (panel b), **11** (panel c), **15** (panel d) at their respective IC_{50s} for 24 h. The diagrams show the distribution of the cells according to their DNA content. The inserts give the percentages of cells in different cell cycle phases.

are in excellent agreement with our notion that the compounds employed affect the redox status of the cell. Redox modulation as the most likely mode of action of our compounds is also in line with the other cell-based assays performed as part of this study.

3. Conclusion

This study has shown a promising synthetic avenue able to generate, with comparable ease, a wide range of tailor-made multifunctional catalysts designed to target cancer cells under OS. The use of simple, straight forward, yet effective multi-component reactions has elegantly cleared the way for the synthesis of tri- and tetra-functional redox agents containing multiple chalcogen, porphyrin metal binding, and quinone redox sites. In addition, the implementation of all combinations of P-3CR with rather flexible building blocks supports the great potential of this concept toward the diversity-oriented synthesis of multifunctional agents. Such agents inhibit proliferation and induce cell death *via* multifactorial mechanisms, such as induction of oxidative stress, cell cycle delay, and apoptosis. Although one can only speculate about the exact mode(s) of biochemical action of these compounds, the presence of several redox sites in these molecules points toward a modulation of the intracellular redox state in these cells.

Quinones are known to increase ROS production in cells, while selenium compounds may 'use' ROS to oxidize and hence impair or inhibit proteins and enzymes. It is likely that a combination of a 'ROS generator' and a 'ROS user' is effective in increasing levels and severity of OS in cells and, in the case of cancer cells, pushes them over the critical ROS threshold. In contrast, normal cells with comparably low intrinsic levels of OS may be less affected. Interestingly, some of the compounds showed no apparent reduction in cell survival when incubated with normal healthy cells, and it is therefore possible that such compounds may have a selective anticancer activity.

Indeed, a chain of biochemical events is emerging, which leads from our redox modulating compounds to ROS generation, reduction of GSH levels and OS, and subsequently to cell cycle arrest and induction of apoptosis. These events seem to occur primarily in cells with a pre-existing disturbance in their intracellular redox balance, such as certain cancer cells.

Our studies provide ample opportunities for future research at the chemistry/biology interface. As far as synthetic chemistry is concerned, future studies may refine and expand the method proposed here, building upon more – and more diverse – building blocks, most of which will be easily accessible. At the same time, there is a need for more chemically diverse catalytic compounds. Here, the development of such multifunctional catalysts is not just dictated by an interest in anticancer drugs. It also poses a real challenge to synthetic organic chemistry, which needs to employ a sophisticated arsenal of modern synthetic techniques to deal with

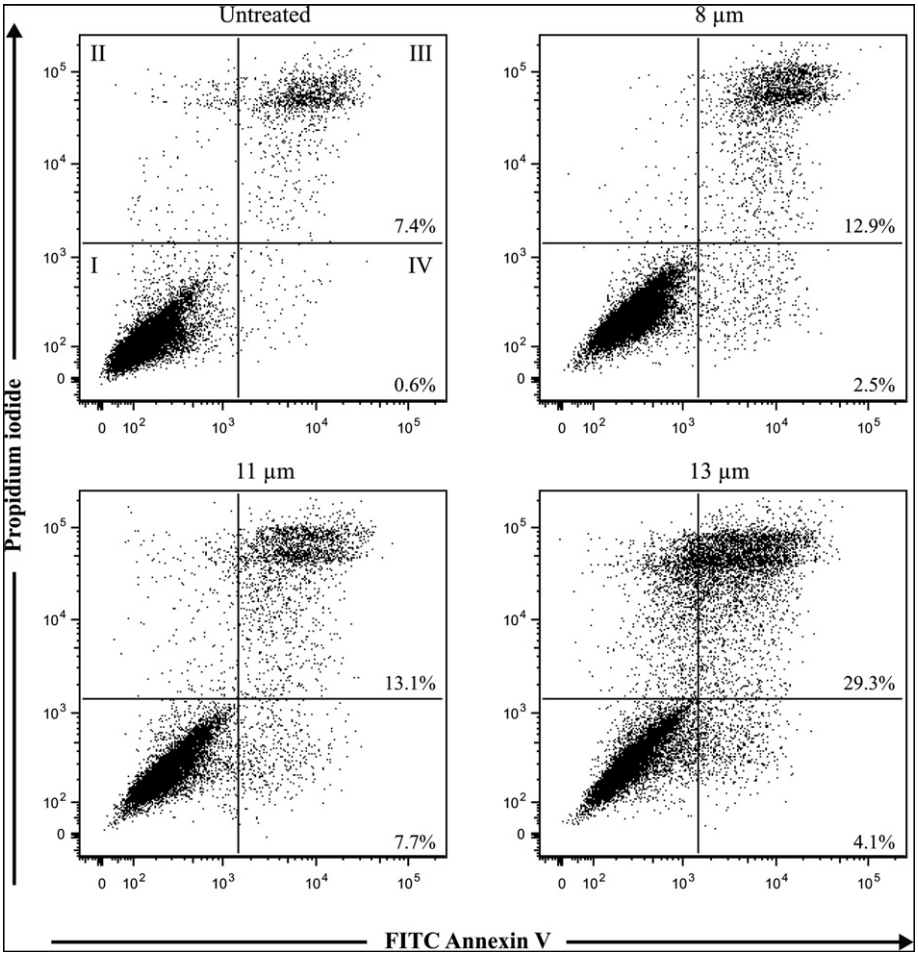

Fig. 7. Flow cytometric analysis of apoptosis. A-431 melanoma cells were treated with 0, 8, 11, and 13 μM of compound **15** for 12 h, and stained with FITC annexin V and propidium iodide. Quadrant I contains the percentage of viable cells (stained neither with PI nor with FITC annexin V); quadrant III shows the percentage of late apoptotic cells (stained with both PI and FITC annexin V), and quadrant IV the percentage of early apoptotic cells (stained with FITC annexin V only).

the relevant quinone and chalcogen chemistry. The synthesis of organoselenium and organotellurium compounds has never been an easy task, and this area of research provides ample opportunities for further development and expansion. Indeed, this study opens the door to a range of follow-up studies in the area of synthetic chemistry, redox chemistry, biochemistry and, ultimately, drug development. Preliminary cell based studies point toward a reasonably selective activity of some of these compounds, which needs to be investigated further by using a considerably wider arsenal of cells. Furthermore, in order to establish the complete picture of redox catalysts as possible therapeutics, this line of investigation will then need to move on to studies in animal models. In any case, there is plenty of scope for further, multi-disciplinary studies involving chemistry, biochemistry, cell biology, and pharmacology in order to develop a strategy to treat cancer by applying redox active compounds.

Table 3
Activity of the multifunctional compounds against *S. cerevisiae* wild type and mutant strains. Diameters (mm) of inhibition zones of an agar diffusion assay are provided. In each case 6 mm disks with 20 μg of the test compound were incubated.

Cpd. no.	BY4741	YJR104C	YHR008C	YDR032C	YHL028W	YLL060C	YPL188W	YGL158W	YOL049W	YLL009C	YDL190C
	Control	SOD1	SOD2	PST2	WSC4	GTT2	POS5	RCK1	GSH2	COX17	UFD2
4	0	10	0	12	11	0	0	0	0	10	10
5	0	15	12	12	11	12	9	9	9	0	0
6	0	18	13	12	12	0	0	0	0	0	0
8	0	13	12	11	11	17	0	0	0	0	0
9	0	16	15	11	16	12	10	10	10	11	0
10	0	22	19	11	19	21	11	18	18	13	13
11	0	21	18	11	20	20	11	14	14	14	0
12	0	17	11	15	0	12	0	0	0	0	0
13	0	20	25	11	14	18	0	0	0	0	0
14	0	12	0	11	14	12	0	0	0	0	0
15	0	14	19	16	26	25	17	15	15	15	15

At the end, this is one of the first studies on a vastly unknown class of compounds and hence it is too early to report on metabolic studies, pharmacokinetics in animals and enrichment of such compounds in specific tissues or degradation. Nonetheless, these issues are clearly important and will form part of future studies in appropriate animal models.

4. Experimental protocols

4.1. Material and methods

All chemical reagents for the synthesis of compounds were purchased from Sigma–Aldrich–Fluka and used without further purification unless stated otherwise. Reactions under inert atmosphere were carried out under argon (4.6) using standard Schlenk techniques. Silica gel 60 (Macherey–Nagel, 50–200 μm) was used for column chromatography. Unless noted otherwise, the dimensions of columns used were 2.5 cm (diameter) and 25–30 cm (height of silica gel). TLC plates (silica gel 60 F_{254}, 0.20 mm) were purchased from Merck. NMR Spectroscopy: ^{1}H NMR spectra were recorded at 500 MHz, ^{13}C NMR spectra at 125 MHz on a Bruker DRX 500 or Avance 500 spectrometer. Chemical shifts are reported in δ (ppm), expressed relative to the solvent signal at 7.26 ppm ($CDCl_3$, ^{1}H NMR) and at 77.16 ppm ($CDCl_3$, ^{13}C NMR), as well as 3.31 ppm (^{1}H NMR, CD_3OD) and 49.00 ppm (^{13}C NMR, CD_3OD). Coupling constants (J) are given in Hz. LC–MS/MS analysis: Analyses were performed using a TSQ Quantum mass spectrometer equipped with an ESI source and a triple quadrupole mass detector (Thermo Finnigan). HRMS: High-resolution mass spectrometry was performed on an Accela UPLC-system (Thermo-Fisher) coupled to a linear trap-FT-Orbitrap combination (LTQ-Orbitrap), operating in positive ionization mode. These spectra indicated the ≥95% purity of the prepared compounds.

4.2. Synthesis and characterization

4.2.1. General procedure for the preparation of compounds via the three-component Passerini reaction **4**–**18**

As a general procedure, a mixture of aldehyde (1 mmol), carboxylic acid (1.2 mmol) and isonitrile (1.5 mmol) in 5 mL degassed water was stirred at room temperature overnight. Upon completion (monitored by TLC), 10 mL CH_2Cl_2 was added to dissolve the sticky product. The aqueous layer was washed with CH_2Cl_2 three times, the organic layers were combined, dried over Na_2SO_4 and concentrated to yield a sticky product which was purified by chromatography on silica gel, usually with petrol ether: ethyl acetate (4:1) as eluent. Analytical information for individual compounds is given in the Supplementary material.

Compounds number **5**, **7**, **11**, **15**, and **18** were synthesized according to the literature [9,10].

*4.2.1.1. 1-(tert-Butylcarbamoyl)-3-(phenylselanyl)propyl3-(1,4-dihydro-2-methyl-1,4-dioxonaphthalen-3-ylthio)propanoate (**4**).* Compound **4** was synthesized from 3-(phenylselanyl)propanal (213.1 μL, 1 mmol), 3-(3-methyl-1,4-dioxo-1,4-dihydronaphthalen-2-ylthio)propanoic acid (331.6 mg, 1.2 mmol) and *tert*-butyl isocyanide (124.6 μL, 1.5 mmol). Its formation was monitored by TLC petrol ether: ethyl acetate = 4:1, R_f = 0.63, purified by column chromatography on silica gel with petrol ether: ethyl acetate = 5:1. Yield = 62%. ^{1}H NMR ($CDCl_3$, 500 MHz): δ_{ppm} = 8.03–7.97 (m, 2H), 7.66–7.61 (m, 2H), 7.41–7.38 (m, 2H), 7.17–7.14 (m, 3H), 5.84 (br s, 1H), 5.08–5.06 (t, J = 5.4, 11.8 Hz, 1H), 3.37–3.34 (t, J = 7.3, 13.9 Hz, 2H), 2.86–2.83 (t, J = 7.9, 15.5 Hz, 2H), 2.74–2.71 (m, 2H), 2.27 (s, 3H), 2.18–2.12 (m, 2H), 1.27 (s, 9H) ppm. ^{13}C NMR ($CDCl_3$, 125.79 Hz): δ_{ppm} = 182.0 (s), 181.3 (s), 170.2 (s), 167.7 (s), 147.5 (s), 145.3 (s), 133.8 (d), 133.5 (d), 132.7 (d, 2C), 132.6 (s), 131.9 (s), 129.6 (s), 129.1 (d, 2C), 127.1 (d), 126.8 (d), 126.7 (d), 74.2 (d), 51.5 (s), 35.6 (t), 32.5 (t), 29.1 (t), 28.6 (q, 3C), 22.5 (t), 15.4 (q) ppm. LC–MS (ESI): m/z calc. 573.21, R_t = 14.76 min, m/z found 574.15 $[M + H]^+$. HRMS: [M + H] calc. 574.1141, [M + H] found 574.1161, [M + Na] calc. 596.0130 [M + Na] found 596.0980. Isotopic pattern of selenium: m/z (relative abundance %) 574.1161 (100), 575.1194 (30), 576.1163 (18), 577.1196 (7).

*4.2.1.2. 1-(Benzylhexanoatecarbamoyl)-2-(phenylselanyl)ethyl-3-(1,4-dihydro-2-methyl-1,4-dioxonaphthalen-3-ylthio)propanoate (**6**).* Compound **6** was synthesized from 2-(phenylselanyl)acetaldehyde (200 μL, 1 mmol), 3-(3-methyl-1,4-dioxo-1,4-dihydronaphthalen-2-ylthio)propanoic acid (331.6 mg, 1.2 mmol) and benzyl 6-isocyanohexanoate (346.9 μL, 1.5 mmol). Its formation was monitored by TLC petrol ether: ethyl acetate = 4:1, R_f = 0.35, purified by column chromatography on silica gel with petrol ether: ethyl acetate = 3:1. Yield = 71%. ^{1}H NMR ($CDCl_3$, 500 MHz): δ_{ppm} = 8.02–7.97 (m, 2H), 7.65–7.61 (m, 2H), 7.45–7.41 (m, 2H), 7.29–7.21 (m, 5H), 7.17–7.12 (m, 3H), 6.41 (br t, 1H), 5.37–5.33 (dd, J = 4.4, 5.8 Hz, 1H), 5.00 (s, 2H), 3.41–3.37 (dd, J = 4.4, 13.5 Hz, 1H), 3.28–3.11 (m, 5H), 2.56–2.50 (m, 1H), 2.46–2.40 (m, 1H), 2.27–2.41 (m, 5H), 1.59–1.53 (m, 2H), 1.48–1.42 (m, 2H), 1.31–1.25 (m, 2H) ppm. ^{13}C NMR ($CDCl_3$, 125.79 Hz): δ_{ppm} = 182.3 (s), 181.5 (s), 173.5 (s), 170.2 (s), 168.2 (s), 148.3 (s), 145.5 (s), 136.3 (s), 134.1 (d), 133.7 (d), 133.1 (d, 2C), 132.9 (s), 132.2 (s), 129.8 (s), 129.4 (d, 2C), 128.8 (d, 2C), 128.4 (d), 128.3 (d, 2C), 127.5 (d), 127.6 (d), 126.9 (d), 73.9 (d), 66.4 (t), 39.5 (t), 35.4 (t), 34.2 (t), 29.3 (t, 2C), 29.1 (t), 26.5 (t), 24.6 (t), 15.7 (q) ppm. LC–MS (ESI): m/z calc. 707.146, R_t = 15.16 min, m/z found 708.08 $[M + H]^+$. HRMS: [M + H] calc. 708.1456, [M + H] found 708.1529, [M + Na] calc. 730.1456 [M + Na] found 730.1348. Isotopic pattern of selenium: m/z (relative abundance %) 708.1529 (100), 709.1562 (40), 710.1530 (20), 711.1564 (5), 730.1348 (100), 731.1382 (38), 732.1350 (20), 733.1383 (5).

*4.2.1.3. 1-(Benzylhexanoatecarbamoyl)-3-(phenylselanyl)propyl-3-(1,4-dihydro-2-methyl-1,4-dioxonaphthalen-3-ylthio)propanoate (**8**).* Compound **8** was synthesized from 3-(phenylselanyl)propanal (213.1 μL, 1 mmol), 3-(3-methyl-1,4-dioxo-1,4-dihydronaphthalen-2-ylthio)propanoic acid (331.6 mg, 1.2 mmol) and benzyl 6-isocyanohexanoate (346.9 μL, 1.5 mmol). Its formation was monitored by TLC petrol ether: ethyl acetate = 4:1, R_f = 0.33, purified by column chromatography on silica gel with petrol ether: ethyl acetate = 2.5:1. Yield = 75%. ^{1}H NMR ($CDCl_3$, 500 MHz): δ_{ppm} = 7.99–7.93 (m, 2H), 7.63–7.57 (m, 2H), 7.39–7.35 (m, 2H), 7.27–7.20 (m, 5H), 7.16–7.12 (m, 3H), 6.33 (br s, 1H), 5.19–5.16 (m, 1H), 4.96 (s, 2H), 3.71–3.69 (t, J = 5.4 12.1 Hz, 2H), 3.34–3.30 (t, J = 5.7, 12.4 Hz, 2H), 2.86–2.81 (t, J = 8.0, 15.9 Hz, 2H), 2.76–2.65 (m, 2H), 2.29–2.24 (m, 5H), 2.15–2.09 (m, 2H), 1.56–1.50 (q, J = 7.2, 15.25 Hz, 2H), 1.44–1.38 (q, J = 7.2, 14.8 Hz, 2H), 1.26–1.19 (m, 2H) ppm. ^{13}C NMR ($CDCl_3$, 125.79 Hz): δ_{ppm} = 181.9 (s), 181.3 (s), 173.2 (s), 170.1 (s), 168.6 (s), 147.9 (s), 145.2 (s), 135.9 (s), 133.8 (d), 133.4 (d), 132.7 (d, 2C), 132.5 (s), 132.1 (s), 129.5 (s), 129.1 (d, 2C), 128.4 (d, 2C), 128.1 (d), 128.0 (d, 2C), 127.0 (d), 127.7 (d), 126.6 (d), 73.9 (d), 66.0 (t), 39.0 (t), 35.4 (t), 33.9 (t), 32.5 (t), 29.2 (t), 29.0 (t), 26.1 (t), 24.3 (t), 22.5 (t), 15.3 (q) ppm. LC–MS (ESI): m/z calc. 721.16, R_t = 15.10 min, m/z found 721.94 $[M + H]^+$. HRMS: [M + H] calc. 722.1556, [M + H] found 722.1685, [M + Na] calc. 744.1456 [M + Na] found 744.1505. Isotopic pattern of selenium: m/z (relative abundance %) 722.1685 (100), 723.1719 (39), 724.1687 (18), 725.1721 (6), 744.1505 (100), 745.1538 (36), 746.1506 (16), 747.1540 (5).

*4.2.1.4. 1-(Benzylhexanoatecarbamoyl)-2-(1,4-dihydro-2-methyl-1,4-dioxonaphthalen-3-ylselanyl)ethyl3-(1,4-dihydro-2-methyl-1,4-dioxonaphthalen-3-ylthio)propanoate (**9**).* Compound **9** was

synthesized from 2-(3-methyl-1,4-dioxo-1,4-dihydronaphthalen-2-ylselanyl)acetaldehyde (293 μL, 1 mmol), 3-(3-methyl-1,4-dioxo-1,4-dihydronaphthalen-2-ylthio)propanoic acid (331.6 mg, 1.2 mmol) and benzyl 6-isocyanohexanoate (346.9 μL, 1.5 mmol). Its formation was monitored by TLC petrol ether: ethyl acetate = 4:1, R_f = 0.30, purified by column chromatography on silica gel with petrol ether: ethyl acetate = 2.5:1. Yield = 73%. ^{1}H NMR ($CDCl_3$, 500 MHz): δ_{ppm} = 8.02–7.95 (m, 4H), 7.66–7.56 (m, 4H), 7.30–7.21 (m, 5H), 6.48 (br s, 1H), 5.49–5.46 (m, 1H), 5.01 (s, 2H), 3.69–3.65 (dd, J = 4.5, 13.0 Hz, 1H), 3.50–3.46 (dd, J = 6.2, 13.0 Hz 1H), 3.31–3.23 (m, 2H), 3.19–3.15 (dt, J = 6.7, 13.0 Hz, 2H), 2.67–2.64 (t, J = 6.2, 13.0 Hz, 2H), 2.29–2.24 (m, 8H), 1.58–1.52 (m, 2H), 1.48–1.42 (m, 2H), 1.30–1.18 (m, 2H) ppm. ^{13}C NMR ($CDCl_3$, 125.79 Hz): δ_{ppm} = 182.0 (s), 181.6 (s), 181.3 (s), 181.2 (s), 173.3 (s), 170.0 (s), 167.7 (s), 148.9 (s), 148.0 (s), 145.5 (s), 145.2 (s), 135.9 (s), 133.8 (d), 133.7 (d), 133.5 (d), 133.4 (d), 132.7 (s), 132.6 (s), 131.9 (s), 131.8 (s), 128.5 (d, 2C), 128.2 (d), 128.1 (d, 2C), 127.0 (d), 126.7 (d), 126.6 (d, 2C), 74.1 (d), 66.1 (t), 39.2 (t), 35.4 (t), 34.0 (t), 29.1 (t), 29.0 (t), 28.8 (t), 26.3 (t), 24.4 (t), 17.5 (q), 15.4 (q) ppm. LC–MS (ESI): m/z calc. 801.151, R_t = 17.44 min, m/z found 823.89 $[M + Na]^+$. HRMS: [M + H] calc. 802.1576, [M + H] found 802.1584, [M + Na] calc. 824.1406 [M + Na] found 824.1403. Isotopic pattern of selenium: m/z (relative abundance %) 802.1584 (100), 803.1617 (43), 804.1585 (17), 805.1619 (7), 808.1610 (2), 824.1403 (100), 825.1437 (41), 826.1405 (5), 827.1438 (3).

*4.2.1.5. tert-Butyl(R)-1-((1-(tert-butylcarbamoyl)-2-(1,4-dihydro-2-methyl-1,4-dioxonaphthalen-3-ylselanyl)ethoxy)carbonyl)-2-hydroxyethylcarbamate (**10**).* Compound **10** was synthesized from 2-(3-methyl-1,4-dioxo-1,4-dihydronaphthalen-2-ylselanyl)acetaldehyde (293 μL, 1 mmol), 2-(*tert*-butoxycarbonylamino)-3-hydroxypropanoic acid (246 mg, 1.2 mmol) and *tert*-butyl isocyanide (124.6 μL, 1.5 mmol). Its formation was monitored by TLC petrol ether: ethyl acetate = 4:1, R_f = 0.54, purified by column chromatography on silica gel with petrol ether: ethyl acetate = 2.5:1. Yield = 76% of the two isomers. We separated the two isomers by column chromatography for analytical reasons. Isomer 1: ^{1}H NMR ($CDCl_3$, 500 MHz): δ_{ppm} = 8.05–8.02 (m, 1H), 7.99–7.97 (m, 1H), 7.68–7.62 (m, 2H), 6.64 (br s, 1H), 5.37–5.30 (m, 2H), 4.28 (br d, 1H), 4.16 (br s, 1H), 3.74–3.66 (m, 2H), 3.50 (br t, 1H), 3.31–3.26 (dd, J = 8.3, 13.5 Hz, 1H), 2.29 (s, 3H), 1.37 (s, 9H), 1.29 (s, 9H) ppm. ^{13}C NMR ($CDCl_3$, 125.79 Hz): δ_{ppm} = 182.6 (s), 181.2 (s), 170.3 (s), 167.5 (s), 148.9 (s), 144.8 (s), 134.0 (d), 133.5 (d), 132.6 (s), 132.0 (s), 126.9 (d), 126.8 (d), 80.3 (s), 63.7 (t), 56.1 (s), 52.0 (s), 75.3 (d), 77.3 (d), 28.9 (t), 28.6 (q, 3C), 28.3 (q, 3C), 17.3 (q) ppm. LC–MS (ESI): m/z calc. 582.148, R_t = 12.58 min, m/z found 583.04 $[M + H]^+$. HRMS: [M + H] calc. 583.1523, [M + H] found 583.1553, [M + Na] calc. 605.1306 [M + Na] found 605.1373. Isotopic pattern of selenium: m/z (relative abundance %) 583.1553 (100), 584.1587 (34), 585.1555 (20), 586.1588 (4), 605.1373 (100), 606.1406 (26), 607.1374 (16), 608.1408 (4).

Isomer 2: ^{1}H NMR ($CDCl_3$, 500 MHz): δ_{ppm} = 8.09–8.02 (m, 1H), 8.04–8.02 (m, 1H), 7.79–7.59 (m, 2H), 6.46 (br s, 1H), 5.55–5.32 (m, 2H), 4.25 (br d, 1H), 4.07 (br s, 1H), 3.88–3.70 (m, 2H), 3.50 (br t, 1H), 3.25–3.40 (dd, J = 7.6, 13.2 Hz, 1H), 2.35 (s, 3H), 1.42 (s, 9H), 1.34 (s, 9H) ppm. ^{13}C NMR ($CDCl_3$, 125.79 Hz): δ_{ppm} = 182.4 (s), 181.1 (s), 170.5 (s), 167.1 (s), 148.5 (s), 144.7 (s), 133.9 (d), 132.5 (d), 132.4 (s), 131.9 (s), 127.0 (d), 126.8 (d), 80.8 (s), 75.3 (d), 77.3 (d), 62.9 (t), 56.1 (s), 51.9 (s), 29.7 (t), 28.9 (q, 3C), 28.5 (q, 3C), 17.5 (q) ppm.

*4.2.1.6. tert-Butyl(R)-1-((1-(benzylhexanoatecarbamoyl)-2-(1,4-dihydro-2-methyl-1,4-dioxonaphthalen-3-ylselanyl)ethoxy)carbonyl)-2-hydroxyethylcarbamate (**12**).* Compound **12** was synthesized from 2-(3-methyl-1,4-dioxo-1,4-dihydronaphthalen-2-ylselanyl)acetaldehyde (293 μL, 1 mmol), 2-(*tert*-butoxycarbonylamino)-3-hydroxypropanoic acid (246 mg, 1.2 mmol) and benzyl 6-isocyanohexanoate (346.95 μL, 1.5 mmol). Its formation was monitored by TLC petrol ether: ethyl acetate = 2.5:1, R_f = 0.18, purified by column chromatography on silica gel with petrol ether: ethyl acetate = 2:1. Yield = 75% of the two isomers. We separated the two isomers by column chromatography for analytical reasons. Isomer 1: ^{1}H NMR ($CDCl_3$, 500 MHz): δ_{ppm} = 8.02–7.99 (m, 2H), 7.65–7.60 (m, 2H), 7.29–7.24 (m, 5H), 7.15 (br s, 1H), 5.50–5.45 (m, 2H), 5.05 (s, 2H), 4.25–4.15 (m, 1H), 4.05–3.95 (m, 1H), 3.85–3.65 (m, 2H), 3.45–3.40 (m, 1H), 3.25–3.15 (m, 2H), 2.31–2.38 (m, 5H), 1.57–1.39 (m, 4H), 1.35 (s, 9H), 1.27–1.21 (m, 2H) ppm. ^{13}C NMR ($CDCl_3$, 125.79 Hz): δ_{ppm} = 182.1 (s), 181.3 (s), 174.3 (s), 169.9 (s), 168.1 (s), 153.7 (s), 145.0 (s), 133.8 (d), 133.5 (d), 132.6 (s), 132.0 (s), 130.8 (s), 128.8 (s), 128.6 (d, 2C), 128.3 (d), 128.2 (d, 2C), 127.1 (d), 126.8 (d), 80.4 (s), 74.5 (d), 66.5 (t), 63.7 (t), 56.1 (d), 39.2 (t), 33.9 (t), 28.8 (t), 28.5 (t), 28.3 (q, 3C), 26.0 (t), 24.2 (t), 17.5 (q) ppm. Isomer 2: ^{1}H NMR ($CDCl_3$, 500 MHz): δ_{ppm} = 8.03–7.98 (m, 2H), 7.65–7.60 (m, 2H), 7.30–7.25 (m, 5H), 7.15 (br s, 1H), 5.51–5.41 (m, 2H), 5.05 (s, 2H), 4.30–4.17 (m, 1H), 4.08–4.01 (m, 1H), 3.78–3.71 (m, 2H), 3.50–3.38 (m, 1H), 3.26–3.15 (m, 2H), 2.31–2.25 (m, 5H), 1.56–1.43 (m, 4H), 1.33 (s, 9H), 1.27–1.21 (m, 2H) ppm. ^{13}C NMR ($CDCl_3$, 125.79 Hz): δ_{ppm} = 181.9 (s), 181.3 (s), 174.2 (s), 169.9 (s), 168.0 (s), 155.8 (s), 145.0 (s), 133.8 (d), 133.5 (d), 132.5 (s), 131.9 (s), 130.8 (s, 2C), 128.5 (s), 128.3 (d, 2C), 128.2 (d), 128.2 (d, 2C), 127.1 (d), 126.8 (d), 80.3 (s), 74.5 (d), 66.5 (t), 63.7 (t), 56.1 (d), 39.1 (t), 33.9 (t), 28.9 (t), 28.8 (t), 28.2 (q, 3C), 26.0 (t), 24.2 (t), 17.5 (q) ppm. LC–MS (ESI): m/z calc. 730.20, R_t = 13.53 min, m/z found 730.96 $[M + H]^+$. HRMS: [M + H] calc. 731.2097, [M + H] found 731.2077, [M + Na] calc. 753.1807 [M + Na] found 753.1897. Isotopic pattern of selenium: m/z (relative abundance %) 731.2077 (100), 732.2111 (37), 733.2079 (21), 734.2113 (4), 753.1897 (100), 754.1930 (28), 755.1899 (15), 756.1932 (4).

*4.2.1.7. tert-Butyl((1-(benzylhexanoatecarbamoyl)-2-(1,4-dihydro-2-methyl-1,4-dioxonaphthalen-3-ylselanyl)ethoxy)carbonyl)methylcarbamate (**13**).* Compound **13** was synthesized from 2-(3-methyl-1,4-dioxo-1,4-dihydronaphthalen-2-ylselanyl)acetaldehyde (293 μL, 1 mmol), 2-(*tert*-butoxycarbonylamino)acetic acid (210 mg, 1.2 mmol) and benzyl 6-isocyanohexanoate (346.9 μL, 1.5 mmol). Its formation was monitored by TLC petrol ether: ethyl acetate = 2.5:1, R_f = 0.54, purified by column chromatography on silica gel with petrol ether: ethyl acetate = 2:1. Yield = 66%. ^{1}H NMR ($CDCl_3$, 500 MHz): δ_{ppm} = 8.03–8.00 (m, 2H), 7.66–7.60 (m, 2H), 7.30–7.23 (m, 5H), 6.79 (br s, 1H), 5.53–5.51 (m, 1H), 5.03 (s, 2H), 4.79 (br t, 1H), 3.80–3.63 (m, 3H), 3.50–3.46 (dd, J = 6.9, 13.8 Hz, 1H), 3.21–3.07 (m, 2H), 2.30–2.28 (m, 5H), 1.61–1.55 (m, 2H), 1.50–1.44 (m, 2H), 1.35 (s, 9H), 1.30–1.24 (m, 2H) ppm. ^{13}C NMR ($CDCl_3$, 125.79 Hz): δ_{ppm} = 181.6 (s), 181.3 (s), 173.3 (s), 168.8 (s), 167.6 (s), 156.5 (s), 148.9 (s), 136.4 (s), 133.7 (d), 133.5 (d, 2C), 132.7 (s), 131.9 (s), 128.5 (d, 2C), 128.2 (d, 2C), 126.9 (d), 126.8 (d), 80.6 (s), 74.4 (d), 66.1 (t), 42.3 (t), 39.3 (t), 34.1 (t), 28.9 (t), 28.8 (t), 28.2 (q, 3C), 26.2 (t), 24.4 (t), 17.5 (q) ppm. LC–MS (ESI): m/z calc. 700.19, R_t = 13.83 min, m/z found 701.15 $[M + H]^+$. HRMS: [M + H] calc. 701.1976, [M + H] found 701.1972, [M + Na] calc. 723.1707 [M + Na] found 723.1791. Isotopic pattern of selenium: m/z (relative abundance %) 701.1972 (100), 702.2005 (36), 703.1974 (19), 704.2007 (2), 723.1791 (100), 724.1825 (39), 725.1825 (20), 726.1827 (2).

*4.2.1.8. (2S)-1-(Benzylhexanoatecarbamoyl)-2-(1,4-dihydro-2-methyl-1,4-dioxonaphthalen-3-ylselanyl)ethyl 3-(2-tert-butyldisulfanyl)-2-(pivalamido)propanoate (**14**).* Compound **14** was synthesized from 2-(3-methyl-1,4-dioxo-1,4-dihydronaphthalen-2-ylselanyl)acetaldehyde (293 μL, 1 mmol), 2-(*tert*-butoxycarbonylamino)-3-(*tert*-butyldisulfanyl)propanoic acid (370.8 mg, 1.2 mmol) and benzyl 6-isocyanohexanoate (346.9 μL, 1.5 mmol) following the general procedure described above. Its formation was monitored by TLC petrol ether: ethyl acetate = 2.5:1, R_f = 0.18, purified by column

chromatography on silica gel with petrol ether: ethyl acetate = 2:1. Yield = 85% of the two isomers. We were unable to separate the two isomers by simple column chromatography. ^{1}H NMR ($CDCl_3$, 500 MHz): δ_{ppm} = 8.03–7.99 (m, 2H), 7.65–7.61 (m, 2H), 7.30–7.22 (m, 5H), 7.04 (br s, 1H), 5.48–5.48 (m, 1H), 5.23 (s, 2H), 5.03 (s, 2H), 3.14–3.02 (m, 3H), 2.30–2.26 (m, 6H), 1.60–1.54 (m, 2H), 1.50–1.43 (m, 3H), 1.37 (s, 3H), 1.33 (s, 9H), 1.24 (s, 9H) ppm. ^{13}C NMR ($CDCl_3$, 125.79 Hz): δ_{ppm} = 181.46 (s), 181.3 (s), 170.1 (s), 169.6 (s), 167.6 (s), 148.7 (s), 136.1 (s), 133.7 (d), 133.5 (d), 133.6 (d), 132.8 (s), 132.7 (s), 131.9 (s), 128.5 (d, 2C), 128.2 (d, 2C), 126.9 (d), 126.7 (d), 74.8 (d), 74.5 (d), 66.5 (t), 53.9 (s), 53.4 (s), 48.6 (s), 39.4 (t), 33.3 (t), 34.1 (t), 29.8 (q, 3C), 28.9 (t), 28.3 (q, 3C), 26.3 (t), 24.5 (t, 2C), 17.5 (q) ppm. LC–MS (ESI): *m/z* calc. 818.20, R_t = 16.13 min, *m/z* found 835.02 $[M + NH_4]^+$. HRMS: [M + H] calc. 818.1196, [M + H] found 835.2196, [M + NH_4] calc. 857.2017 [M + K] found 857.2015. Isotopic pattern of selenium: *m/z* (relative abundance %) 835.2196 (100), 836.2229 (47), 837.2197 (20), 840.2189 (2).

*4.2.1.9. 21H,23H-Porphine, 5-(4-((tert-butylcarbamoyl)methyl formate) phenyl)-10,15,20-triphenyl (**16**).* Compound **16** was synthesized from formaldehyde (75 μL, 1 mmol), 5-(4-carboxyphenyl)-10,15,20-triphenylporphyrin (789.0 mg, 1.2 mmol) and *tert*-butyl isocyanide (124.6 μL, 1.5 mmol). TLC, R_f = 0.39 (petroleum ether: ethyl acetate 4:1). It was purified by column chromatography on silica gel with petrol ether: ethyl acetate = 5:2. The compound was obtained as a purple solid. Yield = 93%. ^{1}H NMR (DMSO-d^6, 500 MHz): δ_{ppm} = 8.90–8.88 (m, 6H), 8.80–8.75 (m, 2H), 8.53–8.49 (m, 2H), 8.39–8.25 (m, 2H), 8.24–8.19 (m, 6H), 7.79–7.71 (m, 9H), 6.12 (s, 1H), 4.92 (s, 2H), 1.50 (s, 9H), −2.75 (s, 2H) ppm. ^{13}C NMR (DMSO-d^6, 125.79 Hz): δ_{ppm} = 167.44 (s), 166.0 (s), 149.60 (s), 148.19 (s), 145.72 (s), 142.25 (s, 8C), 134.81 (d), 134.53 (d, 10C), 128.02 (d, 2C), 127.87 (d, 2C), 126.73 (d, 10C), 120.99 (s), 120.70 (s, 4C), 118.17 (s), 77.02 (d, 2C), 52.08 (s), 29.36 (t), 28.79 (q, 3C) ppm. LC–MS (ESI): *m/z* calc. 771.32, R_t = 16.99 min, *m/z* found 772.18 $[M + H]^+$. HRMS: [M + H] calc. 772.3377, [M + H] found 772.3265.

*4.2.1.10. 21H,23H-Porphine, 5-(4-(1-(tert-butylcarbamoyl)-2-(phenylselanyl)ethyl formate)phenyl)-10,15,20-triphenyl (**17**).* Compound **17** was synthesized from 2-(phenylselanyl)acetaldehyde (200 μL, 1 mmol), 5-(4-carboxyphenyl)-10,15,20-triphenylporphyrin (789.0 - mg, 1.2 mmol) and *tert*-butyl isocyanide (124.6 μL, 1.5 mmol). TLC, R_f = 0.51 (petroleum ether: ethyl acetate 4:1). It was purified by column chromatography on silica gel with petrol ether: ethyl acetate = 5:2. The compound was obtained as a purple solid. Yield = 89%. ^{1}H NMR (DMSO-d^6, 500 MHz): δ_{ppm} = 8.98–8.90 (m, 6H), 8.85–8.75 (m, 2H), 8.20–8.35 (m, 10H), 7.82–7.75 (m, 10H), 7.68–7.60 (m, 2H), 7.29–7.35 (m, 2H), 6.15 (s, 1H), 5.75 (t, J = 5.7, 12.4 Hz, 1H), 3.75–3.40 (m, 2H), 1.45 (s, 9H), −2.85 (s, 2H) ppm. ^{13}C NMR (CDCl3, 125.79 Hz): δ_{ppm} = 167.43 (s), 165.35 (s), 165.30 (s), 147.80 (s), 142.01 (s, 10C), 134.66 (d, 4C), 134.53 (d, 10C), 132.99 (d, 2C), 129.74 (s), 129.29 (d, 6C), 128.02 (d), 127.82 (d), 127.32 (s), 126.73 (d, 8C), 120.71 (s, 2C), 120.45 (s, 2C), 74.4 (d), 51.81 (s), 29.08 (t), 28.79 (q, 3C) ppm. LC–MS (ESI): *m/z* calc. 941.28, R_t = 18.40 min, *m/z* found 942.43 $[M + H]^+$. HRMS: [M + H] calc. 942.2937, [M + H] found 942.2917. Isotopic pattern of Se: *m/z* (relative abundance %) 942.2917 (100), 943.2950 (63), 944.2984 (20), 945.2952 (12).

4.3. Biological assays

4.3.1. Cytotoxicity assay

All cell lines were from the DSMZ (Braunschweig, Germany). Human umbilical vein endothelial cells (HUVEC) were from Lonza, human fibroblasts (HF) isolated from foreskin were a generous gift of Dr. Thierauch, Bayer-Schering Pharma AG. All cells were grown at 37 °C and 10% CO_2 in the following media: MCF-7 in DMEM supplemented with 1% L-glutamine and 1% non essential amino acids, A-498 in MEM (Lonza), A-431 in RPMI 1640 (Gibco), HUVEC in EBM-2 (Lonza) and HF in MEM (Gibco) supplemented with 1% L-glutamine. All media were supplemented with 10% fetal calf serum (Lonza or Gibco).

MTT [3-(4,5-dimethylthiazol-2-yl)2,5-diphenyltetrazolium bromide] (Sigma) was used to measure the metabolic activity of cells which are capable of reducing it by dehydrogenases to a violet colored formazan product. Briefly, 120 μL aliquots of a cell suspension (50,000 cells mL^{-1}) in 96-well microplates were incubated at 37 °C and 10% CO_2 and allowed to grow for two days. Then 60 μL of serial dilutions of the test compounds were added. After 24 h of incubation at 37 °C and 10% CO_2, 20 μL MTT in phosphate buffered saline (PBS) were added to a final concentration of 0.5 mg mL^{-1}. After 2 h the precipitate of formazan crystals was centrifuged and the supernatant discarded. The precipitate was washed with 100 μL PBS and dissolved in 100 μL isopropanol containing 0.4% hydrochloric acid. The resulting color was measured at 590 nm using an ELISA plate reader. All investigations were carried out in two parallel experiments. The IC_{50} values were determined as the concentrations of tested materials, which showed 50% of the absorbance of untreated control cells as estimated from the dose–response curves.

4.3.2. In vitro studies

4.3.2.1. DTNB assay as indicative of intracellular GSH concentrations. MCF-7 cells (10^6) were treated with different concentrations of selected test compounds (final concentration 5–20 μM) for 1 h at 37 °C. The cells were removed by mild trypsinizing, centrifuged at 800 rpm for 5 min, washed twice with cold phosphate buffered saline and lysed using 5% w/v chilled metaphosphoric acid at 4 °C for 2 h to extract the cellular GSH. The suspension was then centrifuged at 13,000 rpm for 5 min and GSH determined by the following method. The supernatant was mixed with 0.2 M sodium phosphate buffer (pH 8.0) and 0.04 mM DTNB (5,5′-dithiobis(2-nitrobenzoic acid)) and kept at room temperature for 10 min. The absorbance of the samples was recorded against reagent blank at 412 nm in a UV–vis double beam spectrophotometer (Shimadzu-1640). The GSH levels were calculated from a standard curve prepared with known concentrations of GSH under similar conditions.

4.3.2.2. Detection of ROS generation. The ability of multifunctional redox compounds to induce intracellular ROS formation was determined using DHE and DCF assays. Cells were seeded in 96 wells plates at a density of 10^5 cells per well and treated with different concentrations of the test compounds for 1 h. The cells (180 μL) were then incubated with 20 μL of 10 μM DHE or DCF probes for 30 min in the dark. The fluorescence was immediately read in a fluorescence spectrophotometer (DHE, $\lambda_{ex}/\lambda_{em}$ = 540 ± 25/600 ± 40 nm; DCF, $\lambda_{ex}/\lambda_{em}$ = 485 ± 20/528 ± 20 nm). Results were expressed as arbitrary units per 10^5 cells.

4.3.2.3. Determination of caspase-3/7 activity. The caspase activity was assessed in A-431 cells with the caspase-Glo 3/7 kit (Promega) according to supplier's instruction. Briefly, melanoma cells were seeded in 384-well plates at a density of 20,000 cells per well and treated with 2.8 μM of test compound **15** and allowed to incubate for 1, 2, 4, 6, 12, and 24 h in the dark (37 °C, at 5% CO_2). Caspase-Glo 3/7 reagent was then added and kept at room temperature for further 30 min in the dark. Luminescence of each sample was measured in a plate-reading luminometer.

4.3.2.4. Monitoring phosphatidylserine translocation. Apoptosis was also analyzed by FITC annexin V: propidium iodide staining (BD Biosciences). A-431 cells (10^6) were treated with different

concentrations (0, 8, 11, and 13 μM) of test compound **15** for 12 h. Cells were then trypsinized and washed with PBS. 10^6 cells were suspended in 1 mL binding buffer, then 100 μL were transferred and stained with 5 μL FITC annexin V and 5 μL PI for 15 min. At the end of incubation 400 μL of binding buffer was added and the samples were analyzed by FacScan.

4.3.2.5. Cell cycle analysis. Treated MCF-7 cells (10^6) were fixed with cold (−20 °C) methanol (70%) at 4 °C for one day. Cells were washed with PBS and then treated with saponin (0.1% in PBS). Finally, propidium iodide (500 μL, 20 μg mL^{-1}) and RNAse (1 mg mL^{-1}) were added. After 30 min, samples were analyzed by FacScan.

4.3.2.6. Immunofluorescence microscopy. Cells were grown on cover slips in 4-well plates, test compounds were added after the cells had become semi-confluent and incubated for 24 h. Cells were fixed with 3.7% paraformaldehyde (followed by Triton-X 100 (0.1%) treatment for 5 min) or ice cold methanol/acetone (50:50) for 10 min and then washed with phosphate-buffered saline (PBS). Primary antibodies were added and incubated for 45 min and washed with PBS. Secondary antibodies were then added to the cells and incubated for further 45 min. After washing with PBS, 4′,6-diamidino-2-phenylindole (DAPI) was added and kept at room temperature for 5 min. Cover slips were mounted in anti-fade mounting medium (Molecular Probes). Images were taken with a CCD camera attached to a fluorescence microscope. The following antibodies were used: anti-GRP94, anti- α-tubulin, anti-mouse Alexa Fluor 488 and anti-rat Alexa Fluor 488. The actin filaments were stained with phalloidin Alexa Fluor 594 for 45 min.

4.3.2.7. Agar diffusion assays. Mutants of *S. cerevisiae* (EUROSCARF) were grown on standard YPD medium and seeded into liquid agar medium 90 (see Supplementary material) to a final optical density of 0.1 nm. Paper discs of 6 mm diameter soaked with 20 μL of methanolic solution of the test compounds (1 mg mL^{-1}) were added to the agar plates and incubated at 30 °C. The yeast growth was observed after 1 and 2 days. The diameter of the resulting inhibition zones was given as a measure for antimicrobial activity.

4.3.2.8. Minimal inhibitory concentration (MIC) assay. MIC values were determined with serial dilutions of the compounds that were added to the suspended mutants in liquid media using 96-well microtiter plates. The concentration range of tested compounds was 0.36–50 μg mL^{-1}. The seeded plates were incubated at 30 °C for 24 h, and then the optical density at $\lambda = 620$ nm was recorded on a VICTOR 1420 micro plate reader. MIC was defined as the compound concentration that induces 90% inhibition of growth compared to the control.

4.3.2.9. Screening for chemical–genetic interaction. A mutant library of *S. cerevisiae* consisting of 4800 deletion mutants, generated by the European Archive for Functional Analysis (EUROSCARF), was used to screen for chemical–genetic interactions. 5 μL of each mutant was seeded into wells of 384-well plates with 40 μL/well YPD medium to which 5 μL of compound was added. Liquid handling was carried out by means of an automated pipetting system. The seeded plates were incubated at 30 °C for 24 h, and then the optical density of each well was recorded on a VICTOR 1420 micro plate reader at $\lambda = 620$ nm.

Acknowledgments

The authors thank the Egyptian Ministry of Higher Education, the University of Saarland, the Ministry of Economics and Science of Saarland, and the National Cancer Institute for financial support.

Appendix A. Supplementary material

Supplementary data related to this article can be found at http://dx.doi.org/10.1016/j.ejmech.2012.09.033.

References

[1] O.M. Fischer, S. Streit, S. Hart, A. Ullrich, Beyond Herceptin and Gleevec, Curr. Opin. Chem. Biol. 7 (2003) 490–495.
[2] J.H. Goldie, Drug resistance in cancer: a perspective, Cancer Metastas. Rev. 20 (2001) 63–68.
[3] D. Trachootham, J. Alexandre, P. Huang, Targeting cancer cells by ROS-mediated mechanisms: a radical therapeutic approach? Nat. Rev. Drug Discov. 8 (2009) 579–591.
[4] H. Pelicano, D. Carney, P. Huang, ROS stress in cancer cells and therapeutic implications, Drug Resist. Updat. 7 (2004) 97–110.
[5] A.T.Y. Lau, Y. Wang, J.- Chiu, Reactive oxygen species: current knowledge and applications in cancer research and therapeutic, J. Cell. Biochem. 104 (2008) 657–667.
[6] J. Wang, J. Yi, Cancer cell killing via ROS: to increase or decrease, that is the question, Cancer Biol. Ther. 7 (2008) 1875–1884.
[7] F.H. Fry, C. Jacob, Sensor/effector drug design with potential relevance to cancer, Curr. Pharm. Des. 12 (2006) 4479–4499.
[8] V. Jamier, L.A. Ba, C. Jacob, Selenium- and tellurium-containing multifunctional redox agents as biochemical redox modulators with selective cytotoxicity, Chem. A Eur. J. 16 (2010) 10920–10928.
[9] S. Shabaan, L.A. Ba, M. Abbas, T. Burkholz, A. Denkert, A. Gohr, L.A. Wessjohann, F. Sasse, W. Weber, C. Jacob, Multicomponent reactions for the synthesis of multifunctional agents with activity against cancer cells, Chem. Commun. (Camb) 31 (2009) 4702–4704.
[10] S. Mecklenburg, S. Shaaban, L.A. Ba, T. Burkholz, T. Schneider, B. Diesel, A.K. Kiemer, A. Roseler, K. Becker, J. Reichrath, A. Stark, W. Tilgen, M. Abbas, L.A. Wessjohann, F. Sasse, C. Jacob, Exploring synthetic avenues for the effective synthesis of selenium- and tellurium-containing multifunctional redox agents, Org. Biomol. Chem. 7 (2009) 4753–4762.
[11] D.H. Roos, R.L. Puntel, M.M. Santos, D.O. Souza, M. Farina, C.W. Nogueira, M. Aschner, M.E. Burger, N.B. Barbosa, J.B. Rocha, Guanosine and synthetic organoselenium compounds modulate methylmercury-induced oxidative stress in rat brain cortical slices: involvement of oxidative stress and glutamatergic system, Toxicol. Vitro 23 (2009) 302–307.
[12] R. Naithani, Organoselenium compounds in cancer chemoprevention, Mini Rev. Med. Chem. 8 (2008) 657–668.
[13] A. Bhalla, S. Sharma, K.K. Bhasin, S.S. Bari, Convenient preparation of benzylseleno- and phenylselenoalkanoic acids: reagents for synthesis of organoselenium compounds, Synth. Commun. 37 (2007) 783–793.
[14] I. Akritopoulou-Zanze, Isocyanide-based multicomponent reactions in drug discovery, Curr. Opin. Chem. Biol. 12 (2008) 324–331.
[15] A. Domling, I.I. Ugi, Multicomponent reactions with isocyanides, Angew. Chem. Int. Ed. Engl. 39 (2000) 3168–3210.
[16] M.C. Pirrung, K.D. Sarma, Multicomponent reactions are accelerated in water, J. Am. Chem. Soc. 126 (2004) 444–445.
[17] M.C. Pirrung, K. Das Sarma, J. Wang, Hydrophobicity and mixing effects on select heterogeneous, water-accelerated synthetic reactions, J. Org. Chem. 73 (2008) 8723–8730.
[18] M. Paravidino, R. Scheffelaar, R.F. Schmitz, F.J. Kanter, M.B. Groen, E. Ruijter, R.V. Orru, A flexible six-component reaction to access constrained depsipeptides based on a dihydropyridinone core, J. Org. Chem. 72 (2007) 10239–10242.
[19] B. Kiran Aithal, M.R. Sunil Kumar, B. Nageshwar Rao, N. Udupa, B.S. Satish Rao, Juglone, a naphthoquinone from walnut, exerts cytotoxic and genotoxic effects against cultured melanoma tumor cells, Cell. Biol. Int. 33 (2009) 1039–1049.
[20] M.R. Kumar, K. Aithal, B.N. Rao, N. Udupa, B.S. Rao, Cytotoxic, genotoxic and oxidative stress induced by 1,4-naphthoquinone in B16F1 melanoma tumor cells, Toxicol. Vitro 23 (2009) 242–250.
[21] T.W. Gant, D.N. Rao, R.P. Mason, G.M. Cohen, Redox cycling and sulphydryl arylation; their relative importance in the mechanism of quinone cytotoxicity to isolated hepatocytes, Chem. Biol. Interact. 65 (1988) 157–173.
[22] S. Fernandez Villamil, A.O. Stoppani, M. Dubin, Redox cycling of beta-lapachone and structural analogues in microsomal and cytosol liver preparations, Methods Enzymol. 378 (2004) 67–87.
[23] M. Nakamura, T. Hayashi, One- and two-electron reduction of quinones by rat liver subcellular fractions, J. Biochem. 115 (1994) 1141–1147.
[24] N.M. Giles, N.J. Gutowski, G.I. Giles, C. Jacob, Redox catalysts as sensitisers towards oxidative stress, FEBS Lett. 535 (2003) 179–182.
[25] J. Fang, H. Nakamura, A.K. Iyer, Tumor-targeted induction of oxystress for cancer therapy, J. Drug Target. 15 (2007) 475–486.
[26] N. Kasugai, T. Murase, T. Ohse, S. Nagaoka, H. Kawakami, S. Kubota, Selective cell death by water-soluble Fe-porphyrins with superoxide dismutase (SOD) activity, J. Inorg. Biochem. 91 (2002) 349–355.
[27] O. Huet, C. Cherreau, C. Nicco, L. Dupic, M. Conti, D. Borderie, F. Pene, E. Vicaut, D. Benhamou, J.P. Mira, J. Duranteau, F. Batteux, Pivotal role of glutathione depletion in plasma-induced endothelial oxidative stress during sepsis, Crit. Care Med. 36 (2008) 2328–2334.

[28] C. Debbascb, P.- Pisella, M. De Saint Jean, P. Rat, J.- Warnet, C. Baudouin, Mitochondrial activity and glutathione injury in apoptosis induced by unpreserved and preserved β-blockers on chang conjunctival cells, Invest. Ophthalmol. Vis. Sci. 42 (2001) 2525–2533.
[29] F.Q. Schafer, G.R. Buettner, Redox environment of the cell as viewed through the redox state of the glutathione disulfide/glutathione couple, Free Radic. Biol. Med. 30 (2001) 1191–1212.
[30] M. Karlsson, T. Kurz, U.T. Brunk, S.E. Nilsson, C.I. Frennesson, What does the commonly used DCF test for oxidative stress really show? Biochem. J. 428 (2010) 183–190.
[31] S. Dikalov, K.K. Griendling, D.G. Harrison, Measurement of reactive oxygen species in cardiovascular studies, Hypertension 49 (2007) 717–727.
[32] H. Zhou, X. Liu, L. Liu, Z. Yang, S. Zhang, M. Tang, Y. Tang, Q. Dong, R. Hu, Oxidative stress and apoptosis of human brain microvascular endothelial cells induced by free fatty acids, J. Int. Med. Res. 37 (2009) 1897–1903.
[33] C.C. Wang, Y.M. Chiang, S.C. Sung, Y.L. Hsu, J.K. Chang, P.L. Kuo, Plumbagin induces cell cycle arrest and apoptosis through reactive oxygen species/c-Jun N-terminal kinase pathways in human melanoma A375.S2 cells, Cancer Lett. 259 (2008) 82–98.
[34] T. Ozben, Oxidative stress and apoptosis: impact on cancer therapy, J. Pharm. Sci. 96 (2007) 2181–2196.
[35] I. Dalle-Donne, R. Rossi, A. Milzani, P. Di Simplicio, R. Colombo, The actin cytoskeleton response to oxidants: from small heat shock protein phosphorylation to changes in the redox state of actin itself, Free Radic. Biol. Med. 31 (2001) 1624–1632.
[36] C. Jacob, A. Anwar, The chemistry behind redox regulation with a focus on sulphur redox systems, Physiol. Plant 133 (2008) 469–480.
[37] C. Jacob, G.I. Giles, N.M. Giles, H. Sies, Sulfur and selenium: the role of oxidation state in protein structure and function, Angew. Chem. Int. Ed. Engl. 42 (2003) 4742–4758.
[38] C. Xu, B. Bailly-Maitre, J.C. Reed, Endoplasmic reticulum stress: cell life and death decisions, J. Clin. Invest. 115 (2005) 2656–2664.
[39] D. Upadhyay, W. Chang, K. Wei, M. Gao, G.D. Rosen, Fibroblast growth factor-10 prevents H_2O_2-induced cell cycle arrest by regulation of G1 cyclins and cyclin dependent kinases, FEBS Lett. 581 (2007) 248–252.
[40] H.K. Baumgartner, J.V. Gerasimenko, C. Thorne, L.H. Ashurst, S.L. Barrow, M.A. Chvanov, S. Gillies, D.N. Criddle, A.V. Tepikin, O.H. Petersen, R. Sutton, A.J.M. Watson, O.V. Gerasimenko, Caspase-8-mediated apoptosis induced by oxidative stress is independent of the intrinsic pathway and dependent on cathepsins, Am. J. Physiol. Gastrointest. Liver Physiol. 293 (2007).
[41] J.S. Bair, R. Palchaudhuri, P.J. Hergenrother, Chemistry and biology of deoxynyboquinone, a potent inducer of cancer cell death, J. Am. Chem. Soc. 132 (2010) 5469–5478.
[42] A. Lopez, A.B. Parsons, C. Nislow, G. Giaever, C. Boone, Chemical-genetic approaches for exploring the mode of action of natural products, Prog. Drug Res. 66 (2008) 237–271.